Research Paper

Volume : 2 | Issue : 5 | May 2013 • ISSN No 2277 - 8179

Adaptive LS-estimation and Fault Recovery Procedure for PZT-actuated milli-actuator of Hard Disk Drives

Engineering

KEYWORDS : Servo systems, robust control, tracking systems, Actuators, perfect tracking, Dual-stage actuator, Adaptive control

Y.Bharadwaja — Assistant professor, Dept. Of Electronics and Control Engineering, SVEC, Tirupati-517102, India

ABSTRACT

This paper deals with the servo control methods for Hard Disk Drives by implementing secondary suspension piezoelectric micro actuator which is adaptive LS-estimation and fault recovery procedure for PZT-actuated milli-actuator. In the recent five decades, hard disk drives have been playing an important role in the development of digital technology. The increasing areal density has provided a lot of challenges for the hard disk drive servo control. During the HDD servos, one of the most important parts is servo pattern which is utilized to generate position feedback signals. Thus, the accuracy and precision of servo patterns written by servo track writing process must be emphasized in order to increase the storage density. The concentric self-track writing has been proposed to improve the quality of servo patterns and save the cost of servo track writing. We confirmed that the adaptive estimation method identified the milli-actuator DC-gain precisely and the fault recovery procedure detected the degradation of milli-actuator gain during track-following data reading/ writing operation.

INTRODUCTION

A. Hard disk drive servo systems

Since the commercial usage of magnetic disk drives began in 1956 [1], the hard disk drive (HDD) has been playing an important role in the modern era of digital technology. A hard disk drive is a non-volatile storage device that stores digitally encoded data on rotating rigid platters with magnetic surfaces. As a result, the problem of accessing data on the rapidly rotating disk media has provided a wealth of control challenges. For the operation of accessing data, a typical modern HDD has the basic components [2] as illustrated in Fig. 1. Data are recorded on concentric tracks on the disk which is rotated by the spindle motor. The magnetic heads attached onto the slider read and write data from and to the disk. The slider is bonded to the so-called suspension of the actuator arm which pivots about a ball bearing. Thus, as rotating the actuator of the voice coil motor (VCM), we can position the read/write head onto the desired tracks.

According to the features of accessing data on disk, HDD servo systems mainly involve three kinds of control tasks [3]: track-seeking control, track-following control, and setting control. The head positioning servomechanism moves the read/write head as fast as possible from one track to another when asked by the host system (Track-seeking control).

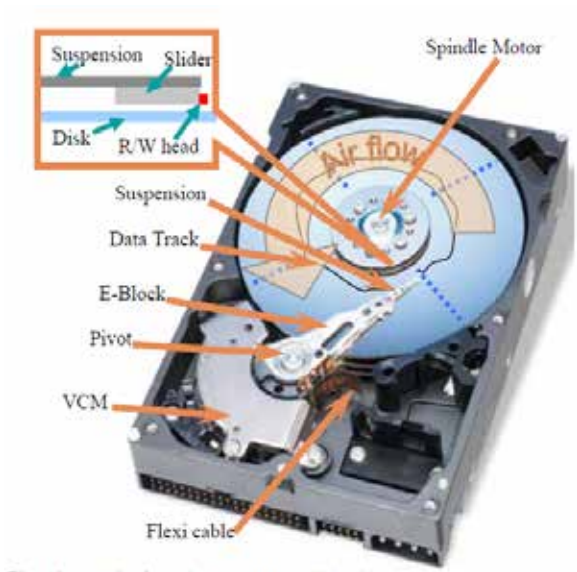

Fig. 1 Schematic of a typical modern hard disk drive.

Once the head reaches the target track, it is regulated over the track so that the head can follows the track as precisely as possible during the operation of reading or writing data (Track following control). Smooth settling, i.e. transition between the track seeking and track following modes without any jerk should be also emphasized in HDD servos.

B. Servo track writing

As discussed in the previous section, the servo patterns, used to generate position feedback signals, must be pre-created. The process of writing servo patterns onto the disk surface at specific locations of servo sectors is known as servo track writing (STW). Since the written servo patterns are utilized to generate the feedback signals for the read/write head position, the accuracy and precision of servo track writing process plays an important role in making the continuously growing trend of track density a reality. For the desired accuracy, there are two critical control problems [9] in the STW process:

1) All patterns required to define the tracks and sectors must be placed in a concentric fashion. Any disturbance and eccentricity present during the process will appear as written-in repeatable run out (RRO) which may degrade the servo performances of the three control tasks.
2) The servo sectors of any track must be precisely aligned with the servo sectors of adjacent tracks. The misalignment results in non-equidistant PES sampling intervals.

In order to improve the precision of servo patterns, the STW process also requires kind of position reference to form a feedback closed-loop control system. According to the different methods used to provide the reference, there have been proposed different kinds of servo track writing techniques, such as conventional servo track writing [10], concentric based self-servo track writing [11], and spiral self-servo track writing [12].

Conventionally, servo patterns are written by costly dedicated servo writing equipment [10] external to disk drives. For example, a laser-guided push-pin mechanism consists of an optical position sensor and controls the position of the write head so that concentric tracks can be created. Besides, in order to precisely align servo patterns along the disk's circumference, a clock track must be firstly written onto the disk and an external clock head is required to read back the timing information from the clock track. Consequentially, the conventional servo writing process needs openings in the drive enclosure to make the external equipment accessible to the media and actuator of the HDD. Moreover, in order to avoid the contamination, it is necessary to carry out the conventional servo writing process in a very clean environment. Besides, as the track density is increasing, the conventional STW using the external equipment is more time-consuming. In order to overcome these drawbacks, the methodologies of self-servo track writing have been developed.

The self-servo track writing (SSTW) process utilizes the HDD's own reading and writing heads and servo system to write servo

patterns without using the external equipment. Thus, the clean room environment is not necessary for the SSTW process, which saves the cost of servo track writing. Besides, with the HDD's own servo system, a self servo writing loop is able to furthermore suppress vibrations via active control, which means the SSTW can improve the quality of servo writing. Currently, there are two kinds of popular SSTW methodologies, i.e. concentric SSTW and spiral SSTW. The concentric SSTW process utilizes the pre-written concentric tracks to write the rest of concentric tracks. And the details of this methodology will be presented in the next section. The spiral SSTW process writes concentric product servo patterns based on the pre-written spirals tracks. The spiral tracks are written by using an external spiral writer, which is less expensive and less time-consuming than the conventional servo track writing process. However, such methodology involves a significant problem that the time of writing final servo patterns may coincide with the time of reading spiral servo information when servoing on spiral servo patterns to write final concentric servo patterns [12].

C. Dual-stage HDD actuator

One of the limitations in the conventional disk drives to achieve higher data capacity is its bandwidth. That is, the voice-coil-motor (VCM) actuator used in conventional disk drives has hundreds of flexible resonant modes in high frequencies. This limits the increase of bandwidth and hence the track density. A possible solution to this kind of problems is to introduce an additional micro actuator on top of the conventional VCM actuator to provide a faster response and thus improve the overall servo performance in the track following stage. In fact, there is a considerable amount of research works that have been done along this line.

Dual-stage actuator refers to the fact that there is a small twin-piezo actuator mounted between the base plate and active suspension of a large conventional VCM actuator. The R/W head is mounted at the end of the active suspension. Fig. 2 shows a simple illustration of a dual-stage actuator considered in this paper. The piezoelectric actuator or micro-actuator, driven by voltage, will only be activated in the track following stage because of its limited movement range. The microactuator produces relative motion of the R/W head along the active suspension or the radial direction in the center of the pivot (see e.g., [6, 9]), while the VCM actuator rotates the base plate and active suspension to move the micro-actuator and the R/W head.

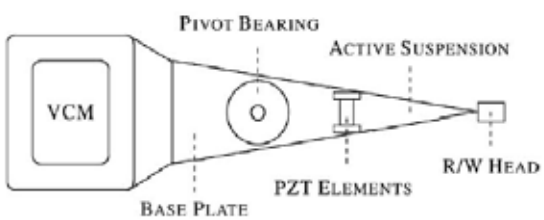

Fig. 2. A dual-stage HDD actuator.

Diverse control strategies and methods have been reported to design the dual stage actuated HDD servo systems. Guo et al. [9] have proposed four control strategies to design the dual-stage actuated control system, which are respectively the so-called parallel loop, master-slave loop, dual feedback loop and master-slave with decoupling methods. Guo et al. [12] and Hu et al.[15] have also utilized the well-known LQG/LTR method to design the dual-stage actuated HDD servo systems. These works have accelerated the progress to improve the HDD servo system performance. But, more studies on the control methods need to be conducted to achieve better results and higher track density in HDD servo systems.

The voice coil motor (VCM) is used in the first stage to generate large but coarse and slow movement, while the micro/milli-actuator is used in the secondary stage to provide fine and fast positioning. The mechanism for positioning the dual-stage actuator can improve both the track-following and the track-seeking performance. In the moving suspension type of dual-stage actuator [4] (see figure-3), the milli-actuator is located between the head suspension and the base-plate, which is moved by the VCM actuator. Each head is moved by each milli-actuator and each milli-actuator consists of two push-pull piezoelectric (PZT) elements. Usually, as the milli-actuator does not have a relative distance sensor output and only the head position output is detectable; the total plant of the dual stage actuator is a double-input single-output (DISO) system. In order to obtain accurate track-following and high-speed track-seeking performance, it is important to identify an accurate value of the PZT gain of each milli-actuator. Moreover, in maintaining performance, it is important to detect degradation of the PZT gain and inform the host system of the possibility actuator failure. Since the conventional adaptation method [6], [7] cannot be easily applied to the DISO system; no research has been done about an adaptive control for the milli-actuator of the DISO system. In the moving slider-type dual-stage actuator, the micro-actuator is located between the suspension and the slider.

The advantage of this type is that the collocation of the actuator and sensor head, so a servo bandwidth of 5 kHz or more, is possible. Some micro-actuators have a relative positioning sensor which indicates the micro-actuator movement distance. If the micro actuator has a relative position, the total plant is a double-input double-output (DIDO) system and the adaptation for the micro-actuator can be easily achieved using the relative position.

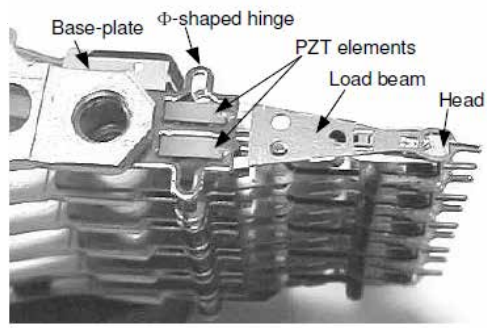

Fig. 3. Moving-suspension type dual-stage actuator

In this section, we discuss the design and implementation of an off-line adaptive scheme for estimating the DC-gain of the PZT actuated milli-actuator for a double-input single output (DISO) system.

A. Moving suspension type dual-stage actuator

Figure 3 shows Φ-shaped dual-stage milli-actuators [4] attached to each carriage arm. The two PZT elements, polarized in opposite directions, are mounted in parallel on an Φ-shaped base plate hinge with a central beam. The top surfaces of the two PZT elements are electrically connected by a wire and the bottom surfaces of each PZT element are adhesively bonded to the base-plate hinge. When a voltage is applied to both single-ended PZT elements, one PZT element extends, and the other one contracts. The push- pull actuation of the PZT elements moves the head in the off-track direction.

The PZT moving-suspension milli-actuator has the following specifications: mass, 75 mg; suspension length, 14.5 mm; stroke, ±1 μm/±30 V; shock resistance, 3,000 G at 0.2 ms half sine. The PZT elements have dimensions of 2.8×1.0×0.15 mm. The milli-actuators were installed in a 3.5-inch prototype HDD at a rotation speed of 10 krpm. The track pitch is 0.75 μm, and the sampling frequency is about 25 kHz.

In general, when the maximum driving voltage ±30V is applied to the PZT milli-actuator, the head position changes by ±1 μm. However, the relationship between the driving voltage and the moving distance of the head (input-output DC-gain characteristics of the actuator) varies about more than 10% due to variations in the manufacturing process of the piezoelectric elements, variations of the piezoelectric element with time, and environmental conditions such as temperature and humidity [5].

Volume : 2 | Issue : 5 | May 2013 • ISSN No 2277 - 8179

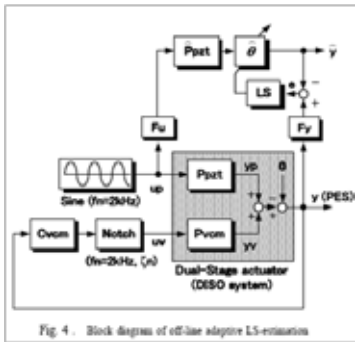

Fig 4 . Block diagram of off-line adaptive LS-estimation

B. VCM loop shaping design for DISO system estimation

Figure 4 shows a block diagram of the adaptive LS estimation system for the milli-actuator with the track following servo system of the VCM actuator.

The dual-stage actuator is operated by two control inputs: a first input u_v to the coarse-movement VCM actuator and a second input u_p to the fine-movement PZT actuator. A head positioning signal y indicating the total movement of the head, obtained by adding the movement of the VCM actuator y_v to that of the PZT actuator y_p, is outputted as an output signal. As a matter of fact, the deviation of the head movement from position information which has previously been recorded on the disk is detected as the Position Error Signal (PES). Thus, the dual-stage actuator is a double input and single-output (DISO) system and it is difficult to implement a conventional adaptive estimation method [6], [7] of a single-input single-output (SISO) VCM actuator in the DISO system.

As for the VCM actuator, its input-output characteristics can be estimated easily using conventional identification methods, by interrupting the driving voltage to the PZT actuator and letting the VCM actuator operate alone. On the other hand, for the estimation of the input-output characteristics of the PZT actuator, it is difficult to let the PZT actuator operate alone in the positioning without the VCM actuator operation, since the stroke of the milli-actuator is too small relative to various external disturbances to the actuator. Therefore, only the PES (total movement of the VCM and PZT actuator) can be used for the adaptive estimation.

The adaptive LS (least-squares) estimation system in Figure 4 identifies the mill-actuator gain precisely using the PES (y) and the PZT input signal u_p with excitation of sine input ($\pm g_o \sin(2\pi f_n . k)$), while the head does not read/write the data. The transfer function from the PZT input u_p to the head position y is described as,

$$y = \frac{1}{1+P_{vcm}C_{vcm}} P_{pzt} . u_p \quad (1)$$

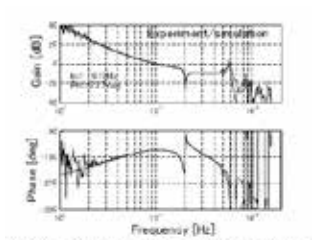

Fig. 5. Frequency response of VCM open loop for off-line adaptation

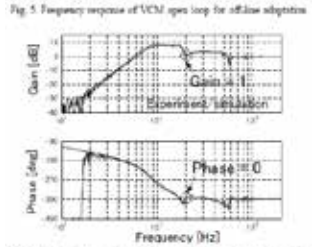

Fig.6. Frequency response of VCM error rejection for off-line adaptation

In order to reject the interference of the VCM servo loop characteristic during the estimation, the notch filter is set in the VCM loop to shape the VCM error rejection $1/(1+P_{vcm}C_{vcm})$ (from y_p to y) into gain 1 (0 dB) at a specific sine-wave frequency fn for PZT actuator. From the viewpoint of the stability and time transient response of the VCM loop, the crossover frequency of the open loop is set to 1 kHz, the cut off frequency of the notch filter is set to 2 kHz and the damping ratio of the notch filter is set to 0.1. **Figure 5** shows both simulation and experiment of the VCM open loop characteristics. The crossover frequency is 1 kHz and the phase margin is 24 degrees. **Figure 6** shows the error rejection characteristics of the VCM loop. The figures indicate that the gain of the VCM error rejection is 1 (0 db) and the phase is 0 degrees at a frequency of 2 kHz which is the same frequency as the PZT actuated frequency f_n during the estimation period.

Thus, the relationship between u_p and y (eq. (1)) can be expressed by the simple equation, where

$$y = P_{pzt} . u_p \text{ at } f_n \text{ (2 kHz frequency)} \quad (2)$$

and we can use the conventional LS-estimation method for the above equation as described below.

C. Adaptive LS-estimation design

The recursive LS-estimation method shown in Figure 4 is explained in detail in the following. In order to reject the noise components from the signals u_p and y, the band-pass filter F_u, F_y which cut-off frequency is 2kHz is used for each signal. For the sake of simplicity, the input u_p and output y will also be used after filtering by the same reference expression. A discrete time model of the milli-actuator from input u_p to the output y_p is expressed by the following equation, in which mechanical resonance is ignored. The calculation time delay is modelled by using first-order Pade approximation and the PZT driver characteristics is modelled by using first-order low-pass filter.

$$y_p(k) = \theta \frac{b_1 . z^{-1} + b_0 . z^{-2}}{1 + a_1 . z^{-1} + a_0 . z^{-2}} u_p(k) \quad (3)$$

Where z^{-1} denote the unit delay operator. The unknown loop gain μ of the plant is composed of the gain of the D/A converter, the gain of the PZT driver, the sensing gain of the head position and the gain of the PZT milli-actuator. **Figure 7** shows the experimental milli-actuator dynamics and simulated plant model described by equation (3). In the figure, since the increase value of the milli-actuator gain dynamics at 2 kHz is small, the milli-actuator resonance characteristic can be neglected.

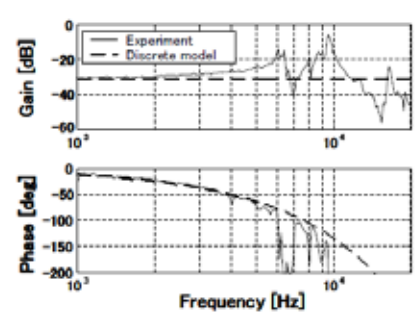

Fig. 7 . Frequency response of exprimental PZT milli-actuator and simulated plant model for estimation

The above equation can be represented as a regression form,

$$y_p(k) = \theta \left(b_1 u(k-1) + b_0 u(k-2)\right) + \left(-a_1 y_p(k-1) - a_0 y_p(k-2)\right) \quad (4)$$

$$= \theta . \zeta(k) + \eta(k).$$

The goal is to estimate a variable gain as a good estimation of the loop gain from $y_p(k)$, (k) and . Here, the estimation of is carried out by use of the recursive least-squares (LS) method. Incidentally, $y_p(k)$ and the head position error $y(k)$ become equal

to each other after a certain length of time. Therefore, can be estimated by using an observable signal $y(k)$ assuming $y_p(k) = y(k)$ in the above expression.

For the estimation expression (3), an estimator model and estimation error are described as,

$$\hat{y} = \hat{\theta}(k-1).\zeta(k) + \eta(k), \quad (5)$$

$$e(k) = y(k) - \hat{y}(k). \quad (6)$$

The recursive adaptive adjustment rule updates the gain estimation value) using the following algorithm [6], [9],

$$\hat{\theta}(k) = \hat{\theta}(k-1) + \frac{\gamma(k-1).\zeta(k)}{1+\gamma(k-1).\zeta(k)^2} e(k) \quad (7)$$

$$\gamma(k) = \frac{\gamma(k-1)}{1+\gamma(k-1).\zeta(k)^2} \quad (8)$$

Where the initial estimation value is = 0 and the initial learning gain is set to (0) > 0.

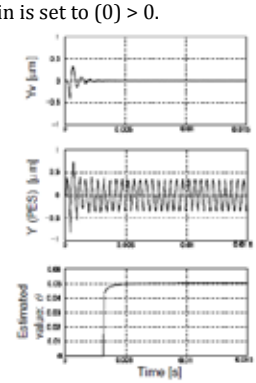

Fig 8. Simulated time response of off-line LS-estimation (VCM position y_v, PES y and estimated value $\hat{\theta}$)

D. Simulation and experimental results

Figure 8 shows the simulated time response waveforms during LS-estimation period. The upper and middle figures show the positions of the output VCM response y_v and the position error signal y, respectively, when a sine wave voltage (±10 V amplitude, 2 kHz frequency) is applied to the milli-actuator. The VCM position y_v responds with a sine wave-like signal until 0.003 sec due to transient of the notch filter and then converges to zero. This means that observed y perfectly coincides with milli-actuator response y_p from 0.003 sec forward. The bottom figure shows the estimated gain value by the LS-estimation which was started at 0.003 sec. The estimated value converged on a correct value in a short time with high accuracy.

The developed off-line LS-estimation method was implemented on a 3.5-inch prototype HDD (10k rpm disk rotation speed) with a moving suspension-type ϕ-shaped milli-actuator (see Fig. 3). **Figure 9** shows the 300 exposed time responses during the estimation period (6 disk revolutions: 36 ms). The head position y moves ± 0.2 μm when the sine wave voltage (±6 V amplitude, 2 kHz frequency) is applied to the milli-actuator. The estimated value converged on a correct value in 10 ms. we measured estimation value 1000 times on each different head at different input voltages from 3 V to 22 V. The estimated variation with 3 deviation is within 1.0% value of its actual value as shown in **Figure 10.**

REAL-TIME GAIN ESTIMATION AND FAULT RECOVERY PROCEDURE

The goal of the second design is to enable an online adaptive estimation method which estimates the input-output characteristics of the PZT milli-actuator and detects its gain degradation even in the midst of data reading/writing. When degradation of the milli-actuator gain is detected, the off-line adaptive gain estimation described in previous chapter will be executed to obtain a precise value of the mill-actuator gain again and set the appropriate value into PZT controller. Thus, the system can keep its servo performance and reliability in the HDD.

A. Adaptive real-time estimation design

An adaptive real-time estimation method for milli-actuator DC-gain degradation is presented. In this scheme, a gain estimator identifies the loop gain of the milli-actuator during the R/W track following phase, and determines the amount of degradation for each PZT gain. **Figure 11** shows the block diagram of the real-time PZT gain estimation method without injection of any external signal. The dual-stage actuator (DISO system) is stabilized by the decoupled type controller [2] in this application. The output of a milli-actuator model M_{pzt} is added into an additional reference signal for the VCM actuator, which prevents the PZT actuator from going to the end of its stroke limit and maintains the PZT output on the centre of the track. The crossover frequency of the milli-actuator is set at 2.3 kHz.

In the figure, the estimated output signal of PZT milli-actuator P_{pzt} *is* calculated by subtracting the output signal of the VCM actuator model $_{vcm}$ from the head position signal y. The VCM model described in the discrete time expression is composed of a second-order low-pass filter. For real-time calculation, the calculation load should be minimized. The adaptive gradient method [9] which cost function J with equation (6) is defined as below is used for gain estimation.

$$J(k) = e^2(k) \quad (9)$$

By using partial differentiation of the above cost function, the gradient estimate equation with the variable gain is obtained as follows,

$$\hat{\theta}(k) = \hat{\theta}(k-1) - \sigma \frac{\partial J(k)}{\partial \hat{\theta}(k)}$$

$$= \hat{\theta}(k-1) + 2\sigma.\zeta(k).e(k) \quad (10)$$

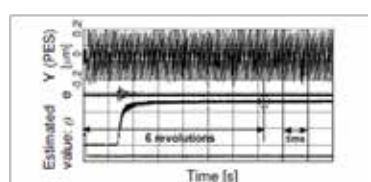

Fig 9. Experimental exposed time response of off-line LS-estimation (PES y, estimated error e and estimated value $\hat{\theta}$)

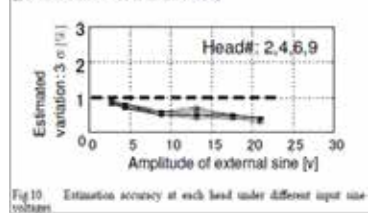

Fig 10. Estimation accuracy at each head under different input sine voltages

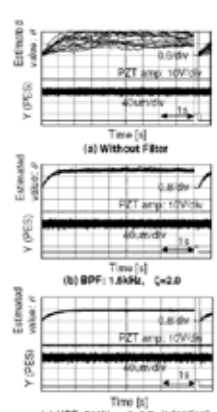

Fig. 11. Experimental exposed time response of real-time gradient estimation with notch noise rejection filter at different disk location (estimated value $\hat{\theta}$ and PES y)

Volume : 2 | Issue : 5 | May 2013 • ISSN No 2277 - 8179

Where denotes the learning gain. The amount of calculation by the above equation is extremely smaller in comparison with the equation (7) and (8). On the other hand, estimation accuracy and/or estimation speed might deteriorate slightly.

B. Simulation and experimental results

The three designs of noise rejecting filter F_u and F_y *in* Figure 11 are evaluated in terms of estimation value and estimation variance. In order to reject the disturbances contaminating the head position signal *y* and the modeling error of $_{vcm}$ and $_{pzt}$, the second-order band-pass filter at 1.5 kHz (= 2:0), the second-order high-pass filter at

700 Hz (= 0:7) and without filter (gain=1) are designed as shown in **Figure 12**. The estimation was carried out at three different locations (inner/middle/outer disk). **Figure 13** shows the time responses of the estimation value and position signal *y* during estimation for evaluating each noise rejection filter. In the case where there was no filter and there was a band-pass filter, the each estimation variation is large depending on the head location. Using the second order high-pass filter we can rejects more low frequency.

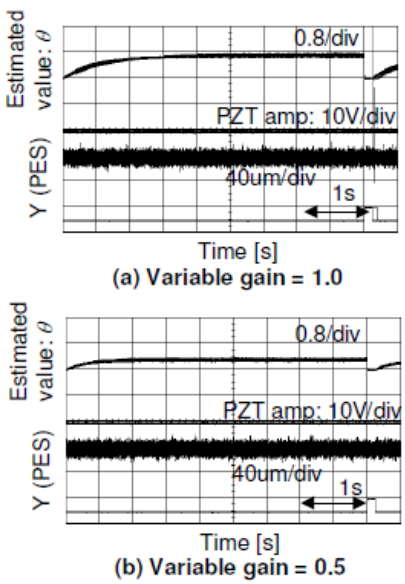

Fig. 14 . Exprimental time response of real-time gradient-estimation under DC-gain change from nominal to half value

VCM input components for force disturbances, a small estimation variation (less than 5% in 3¾) is achieved and the filter is adopted for evaluation. The estimation time is about 1.5 sec. The convergence speed is slower than that in the off-line LS-estimation. However, no particular problem arises when the degradation of the milli-actuator with time is estimated. In **Figure 14**, the accuracy of estimation can be seen when the gain of the milli-actuator was intentionally changed from 1.0 to 0.5. The gradient estimator identified the gain change correctly during the track following mode.

C. Fault recovery for milli-actuator gain degradation

Figure 15 is a flow chart showing a fault recovery process is carried out when the milli-actuator gain drop is detected by the real-time estimation (equation (10)). When a estimated gain drop below a preset threshold value is detected, data reading/writing by the head is prohibited and thereafter the gain of the milli-actuator is estimated correctly according to the off-line LS-estimation method (equations (7)(8)). Subsequently, the estimate value obtained by the LS-estimation is compared with the threshold value. If the difference between the estimated value and the threshold value is small, the milli-actuator controller C_{pzt} is adjusted based on the estimation result. Thereafter, a flag permitting the data read/write is turned on and the dual stage actuator track following returns to its normal state. On the other hand, if the difference between the estimated value and the threshold value is large, an alarm is issued to the upper level holst controller. In such cases of gain drop below the threshold value, the data reading/writing might become impossible, and there is a possibility of failure of the milli-actuator caused by some factors.

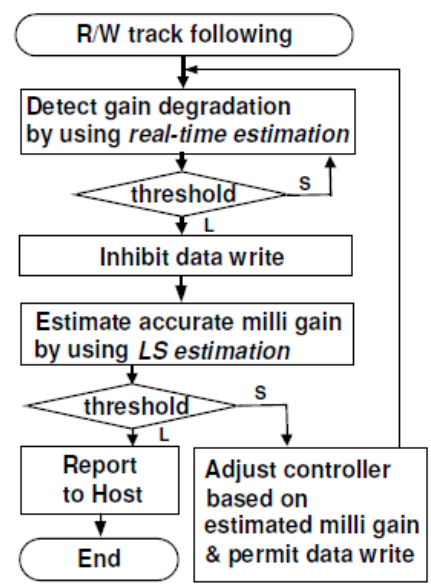

Fig. 15 . Fault recovery flow chart for dual-stage actuator gain degradation

CONCLUSIONS

The design and implementation of adaptive estimation method and a fault recovery scheme for a PZT-actuated milli-actuator were presented. We confirmed that the off-line adaptive LS-estimation method identified the milli-actuator DC-gain precisely within 1.0% value (3 of its actual value in 36 ms. we also confirmed that the fault recovery method detected the degradation of milli-actuator gain within 5.0% value in 1.5 sec and collected the gain properly.

REFERENCE

[1] L. Stevens, "Data storage on magnetic disks," Magnetic Recording: The First 100 Years. E. Daniel, C. Mee, and M. Clark, Eds. Piscataway, NJ: IEEE Press, pp. 270-299, 1997. | [2] B. Chen, T. Lee, and V. Venkataramanan, "Hard Disk Drive Servo Systems," Advances in Industrial Control Series, Springer, New Your, 2006. | [3] D. Abramovitch and G. Franklin, "A brief history of disk drive control," IEEE Control Systems Magazine, vol. 22, no. 3, pp. 28-42, 2002. | [4] E. Rich and D. Curran, "Major HDD TMR Sources and Projected Scaling with TPI," IEEE Trans. On Magnetics, vol. 35, no. 2, pp. 885-891, 1999. | [5] Y. Li and R. Horowitz, "Mechatronics of electrostatic microactuators for computer disk drive dual-stage servo systems," IEEE/ASME Trans. Mechatronics, vol. 6, pp. 988-992, 2001. | [6] S. Felix, J. Nie and R. Horowitz, "Enhanced vibration suppression in HDDs using instrumented suspensions," IEEE Trans. On Magnetics, vol. 45, no. 11, pp. 5118-5122, 2009. | [7] K. Oldham, X. Huang and R. Horowitz, "Design, Fabrication, and Control of a High-Aspect Ratio Microactuator for Vibration Suppression in a Hard Disk Drive," Proceedings of the 16th IFAC Word Congress, Prague, Czech Republic, July 4-8, 2005. | [8] X. Huang and R. Horowitz, "Robust controller design of a dual-stage disk drive servo system with an instrumented suspension," IEEE Trans. On Magnetics, vol. 41, no. 8, pp. 2406-2413, 2005. | [9] A. A. Mamun, G. Guo, and C. Bi, "Hard disk drive: mechatronics and control," Automation and control engineering, Boca Raton, FL, CRC Press, c2007. | [10] Y. Uematsu, M. Fukushi, and K. Taniguchi, "Development of the pushpin free STW," IEEE Trans. On Magnetics, vol. 37, no. 2, pp. 964-968, 2001. | [11] H. Ye, V. Sng, C. Du, J. Zhang, and G. Guo, "Radial error propagation issues in self servo track writing technology," IEEE Trans. On Magnetics, vol. 38, no. 5, pp. 2180-2182, 2002. | [12] D. Brunnett, Y. Sun, and L. Guo, "Method and apparatus for performing a self-servo write operation in a disk drive using spiral servo information," U.S. Patent 7230789B1, Jun., 2007. | [13] D. Cribbs, M. Ellenberger, and J. Hassler, "self-servo writing disk drive and method," U.S. Patent 5448429, 1995. | [14] D. Abramovitch, T. Hurst, and D. Henze, "An overview of the PES Pareto method for decomposing baseline noise sources in hard disk position error signals," IEEE Trans. On Magnetics, vol. 34, no. 1, pp. 17-23, 1998. | [15] T. Ciftcibasi and O. Yuksel, "Sufficient or necessary conditions for modal controllability and observability of Roesser's 2-D system model," IEEE Trans. On Automatic Control, vol. AC-28, no. 4, pp. 527-529, 1983. | [16] H. N. Melkote, R. McNab, B. Cloke, and V. Agarwal, "A study of radial error propagation and self-servowriting in disk drives," in Proceedings of 2002 American Control Conference, 2002, pp. 1372-1377. | [17] C. Du, L. Xie, J. N. Teoh, and G. Guo, "H2 Control for Head Positioning in Axial and Radial Dimensions for Self-Servo Track Writing," IEEE Trans. on Control Systems Technology, vol. 16, No. 1, pp. 177-181, January 2008. | [18] C. Du, L. Xie, and C. Zhang, "H∞ control and robust stabilization of two-dimensional systems in Roesser models," Automatica, vol. 37, no. 2, pp. 205-211, 2001. | [19] R. Yang, L. Xie, and C. Zhang, "H2 and robust H2/H∞ control of 2-D systems in Roesser model," Automatica, vol. 42, no. 9, Sept. 2006. | [20] C. Du, J. Zhang, and G. Guo, "Disturbance Modeling and Control Design for Self-Servo Track Writing," IEEE Trans. On Mechatronics, vol. 10, no. 1, pp. 122-127, Feb. 2005 | [21] T. Semba, T. Hirano, J. Hong and L.S. Fan, "Dual-stage servo controller for HDD using MEMS microactuator,"IEEE Trans. On Magnetics, vol.35, no.5, pp.2271-2273, 1999.